URTeC: 4492424

Applications of Numerical Modeling to Develop Insights into RTA Interpretation

Benson Lamidi*[1], Mouin Almasoodi[5], Mohsen Babazadeh[6], Amanda Baldwin[5], Yalda Barzin[3], Mark Dunseith[2], Craig L. Cipolla[1], Michael McKimmy[7], Andrew Tucker[4], Mohit Paryani[4], Mojtaba Shahri[3], and Mark McClure[1]

[1]ResFrac Corporation, [2]Continental Resources, [3]ExxonMobil Upstream Oil and Gas, [4]APA Corporation, [5]Devon Energy, [6]ConocoPhillips Company, [7]Chevron U.S.A. Inc.

This paper was prepared for presentation at the Unconventional Resources Technology Conference held in Houston, Texas, USA, 22-24 June 2026.

Abstract

In this study, we integrated numerical modeling and field data to investigate several topics related to Rate-Transient Analysis (RTA) in unconventional wells. First, we tested the accuracy of conventional RTA techniques against synthetic data generated by an integrated hydraulic fracturing and reservoir simulator. As expected, pseudopressure adjustments were able to account for sources of nonlinearity such as multiphase flow and pressure-dependent permeability, and they yielded accurate estimates for the linear flow parameter (LFP), fluid in place, and permeability. Two different methods of estimating permeability were assessed, and one proved much more robust than the other. Second, we evaluated whether to perform the analysis with respect to total fluids or with respect to the primary hydrocarbon phase. Results suggest that in some datasets, performing the analysis with respect to total fluids will better capture the character of the RTA transient. The 'total fluids' approach is valuable if linear flow at early time is distorted by changing water cut during early production. Third, we investigated the effect of finite fracture conductivity on RTA behavior. In theory, RTA can be used to identify finite fracture conductivity from the y-intercept on a reciprocal productivity index plot. However, in practice, a clearly discernible y-intercept will only be evident if the conductivity is exceptionally low. Otherwise, the y-intercept can be obscured by the ambiguity created by pressure charging from the hydraulic fracturing treatment. With realistic fracture conductivity values, the fracture is finite conductivity, and yet, in many cases, a y-intercept is not clearly discernable. Fourth, we investigated how to diagnose reservoir behaviors from RTA and GOR plots. Drawing on results from simulations, we made schematic diagrams showing RTA and GOR trends under different conditions. These guidelines can be used for engineering diagnosis of subsurface processes and to guide history matching procedures.

Introduction

Purpose and scope

Rate-transient analysis (RTA) integrates production and pressure data to quantify well productivity and infer reservoir properties. In this study, we used numerical simulation and field datasets to investigate several topics related to RTA interpretation. Analysis was performed on both: (a) simplified 'synthetic' scenarios and (b) simulations based on detailed history matches to historical data (previously presented by Singh et al., 2025, and Morsy et al., 2025). The RTA results were compared with the 'known' values from the simulations to evaluate accuracy and to address practical questions regarding the interpretation procedure.

This paper focuses on RTA techniques utilizing pseudopressure/time corrections. In recent years, 'numerical RTA' methods have become popular (Bowie and Ewert, 2020). These techniques are more general than classical pseudopressure techniques but are largely based on similar assumptions. Therefore, the results in this paper can be viewed as applicable to either classical or numerical RTA techniques.

Background

Sometimes referred to as "time–rate–pressure" analysis, Rate Transient Analysis (RTA) uses production rates and flowing pressures gathered while a well is producing. These data are analyzed using analytical and semi-analytical reservoir flow models to estimate key reservoir parameters such as the linear flow parameter (LFP) and the original fluid in place (OFIP). RTA has become a widely used diagnostic tool in unconventional reservoirs where production is dominated by long periods of transient flow. Unlike traditional pressure transient analysis, which requires well shut-ins, RTA relies on production data, making it particularly useful for tight reservoirs where pressure buildup tests are often impractical (Blasingame and Lee, 1986; Agarwal et al., 1999).

Modern RTA methods were largely developed through the works of Blasingame, who introduced rate-normalized pressure and time functions that allow production data to be interpreted using concepts originally developed for pressure transient analysis. In particular, the framework developed by Blasingame et al. (1991) made it possible to transform routine production data into diagnostically useful forms for flow-regime identification and reserve estimation. Building on this foundation, Agarwal et al. (1999) proposed practical diagnostic approaches that enable the identification of flow regimes directly from production data. For unconventional reservoirs, this framework is especially valuable during transient linear flow. The theoretical basis of the linear-flow straight line (Linear Flow Parameter) originates from the one-dimensional diffusion solutions of Carslaw and Jaeger (1959), while Wattenbarger (1998) translated this behavior into a practical production-analysis method for fractured tight-gas wells. Under transient linear flow, rate-normalized pressure plotted against the square root of time, or approximately the square root of material-balance time under variable operating conditions, yields a straight line whose slope defines the linear-flow parameter (LFP). In the same transformed domain, the flowing-material-balance relationship provides a dynamic analogue to classical material balance, allowing the intercept response to be used for estimating original fluid in place (OFIP) from flowing production data. In this formulation, the classical material balance concept is extended to flowing wells by replacing average reservoir pressure with a pressure function derived from rate-normalized variables. The intercept of the flowing material balance relationship provides an estimate of the contacted fluid volume, while the slope reflects flow capacity and reservoir geometry. Thus, OFIP estimation from production data is obtained as a natural extension of the FMB framework introduced by Blasingame et al. (1991) and extended by Mattar and McNeil (1998), without requiring well shut-in or static pressure measurements.

More recent advancements in RTA applications, particularly for unconventional reservoirs, have been further developed by Clarkson (2021), who expanded the methodology to better interpret fracture-dominated flow and production behavior in shale and tight formations.

In unconventional reservoirs, RTA has been particularly useful for diagnosing linear flow towards hydraulic fractures, a dominant early-time flow regime in tight formations. During this regime, the relationship between production rate, pressure drop, and the square root of production time allows estimation of the linear flow parameter (LFP), which characterizes fracture-controlled flow capacity. The LFP is commonly derived from “square-root-time” or “rate-normalized pressure” plots and provides insight into fracture conductivity and stimulated reservoir volume. As the well transitions from transient flow into boundary-dominated flow (BDF), including the transitional period, RTA can be used to estimate the minimum contacted reservoir area. When boundary-dominated flow is established, the original fluid in place can be determined, thereby allowing production performance to provide constraint on reservoir volume and total drainage area.

Methods

RTA analysis techniques

Consistent with the RTA concepts described above, production rate and flowing pressure data were analyzed using established Rate Transient Analysis (RTA) workflows to estimate the Linear Flow Parameter (LFP) and the original fluid in place (OFIP). The methodology combined diagnostic plots for flow regime identification with straight-line analytical techniques commonly applied to hydraulically fractured unconventional wells.

First, flow-regime identification was performed using the log-log Bourdet derivative of the rate-normalized pressure (or pseudopressure) with respect to time (material-balance time or material-balance pseudotime). The Bourdet derivative provides a smoothed derivative of the production data, allowing clearer identification of dominant flow regimes such as linear flow and boundary-dominated flow. Identifying the linear flow regime is critical because it represents fracture-controlled flow behavior in tight reservoirs and provides the appropriate period for estimating the LFP.

Once the linear flow regime is identified, the linear flow parameter (LFP) for constant or variable rate (Equation 1), originating from the classical linear diffusion solution presented by Carslaw and Jaeger (1959) and later extended to RTA by Blasingame et al. (1991), is determined using the square-root-of-time straight-line analysis shown in Figure 1. During linear flow, a linear relationship exists between the rate-normalized pressure and the square root of material balance time. The slope of this straight-line trend is used to estimate the LFP, which characterizes fracture-controlled flow capacity and provides insight into the effectiveness of the hydraulic fracture system.

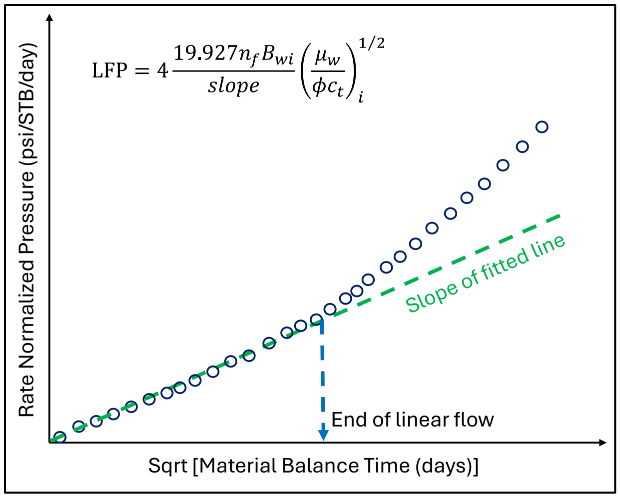

Figure 1: Square-root-of-time straight-line analysis used to estimate the linear flow parameter (LFP). The linear trend during the linear-dominated flow regime is identified, and the slope of the fitted line is used to calculate the LFP

$$LFP = 4\frac{19.927 n_f B_{wi}}{m_{CR}}\left(\frac{\mu_w}{\phi c_t}\right)_i^{1/2} = 4 n_f h x_f \sqrt{k} \tag{1}$$

Here, n_f is the number of effective fractures, B_{wi} is the fluid formation volume factor, μ_w is the fluid viscosity, ϕ is the porosity, m_{CR} is the slope from the fitted line in Figure 1, and c_t is the total effective compressibility.

The original fluid in place (OFIP) is then estimated using the Flowing Material Balance (FMB) method proposed by Mattar and McNeil (1998), as illustrated in Figure 2. This approach relates cumulative production and pressure depletion during boundary-dominated flow to reservoir volume, allowing estimation of the hydrocarbons initially present in the drainage area.

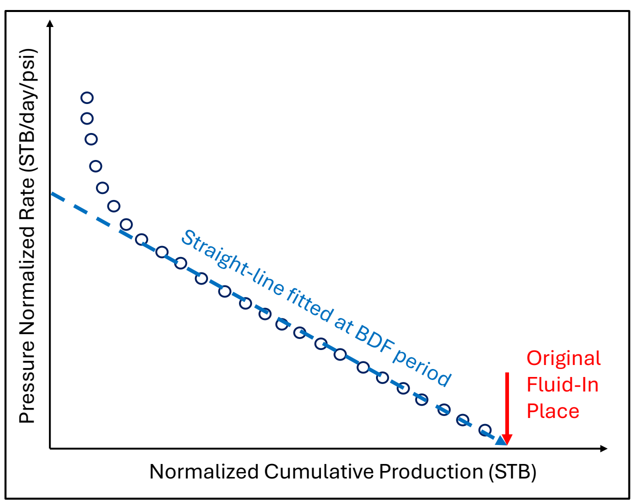

Figure 2: Flowing material balance (FMB) straight-line plot used to estimate original fluid in place (OFIP). The OFIP is obtained from the intercept of the fitted line during the boundary-dominated flow (BDF) period.

Reservoir permeability was subsequently estimated using two RTA-based approaches. In the first approach (Method 1), derived in Equation (2) based on the formulation of Carslaw and Jaeger (1959), Blasingame et al. (1991) and Wattenbarger (1998), permeability was calculated from the time to the end of linear flow (t_{elf}), which relates permeability to reservoir and fracture properties through the duration of the linear flow regime. The time to the end of linear flow (t_{elf}) is determined as the point where the straight-line ends in Figure 1 (point where straight-line begins to deviate upwards). To use this first method, the end of linear flow should be reached. Here, L_w is the effective horizontal length, n_f is number of effective fractures, t_{elf} is the time to end linear flow, μ is the fluid viscosity, ϕ is the porosity and c_t is the total effective compressibility.

$$k = \frac{(\phi\mu c_t)_i}{t_{elf}}\left(\frac{L_w}{0.226 * n_f}\right)^2 \quad (2)$$

In the second approach (Method 2), after boundary dominated flow has reached, permeability is derived using the calculated OFIP and LFP following the formulation of Mattar and McNeil (1998). The OFIP estimate is first used to infer the effective fracture half-length, which is then incorporated into the linear flow parameter relationship to solve for permeability. This method is only applicable during boundary-dominated flow and therefore cannot be used for early-time permeability estimation.

Use the OFIP estimate to back-calculate the effective fracture half-length:

$$OFIP = \frac{2x_f * L_w * h * \phi * S_{wi}}{B_{wi}} \quad (3)$$

Next, use the back-calculated effective fracture half-length to compute permeability from the LFP:

$$LFP = 4n_f h x_f \sqrt{k} \quad (4)$$

Here, k- permeability, ϕ - porosity, n_f- number of effective fractures, $OFIP$ – Original Fluid In-Place, LFP- Linear Flow Parameter, L_w - effective horizontal length, S_{wi} is the initial saturation of the modeled phase, B_{wi} is the phase formation volume factor and h is the reservoir thickness.

The two approaches described above provide independent estimates of permeability, and when consistent pseudo-property corrections are applied, they should yield comparable results under ideal conditions. However, as shown in the results section, these methods often do not yield comparable results under practical conditions.

Finally, the apparent fracture skin and dimensionless fracture conductivity (F_{cd}'), a concept used and studied by Barzin and Mattar (2017), were estimated from the intercept of the square-root-of-time plot (b') as illustrated in Figure 3. The intercept represents the deviation from ideal linear flow behavior and can be related to fracture skin using analytical relationships derived from linear flow solutions. The fracture skin factor was calculated using the intercept-based formulation (Clarkson, 2021):

$$skin = s' = \frac{b' k (2x_f n_f)}{141.2 B_{wi} \mu_{wi}} \quad (5)$$

where k is reservoir permeability, x_f is fracture half-length, B_{wi} is the formation volume factor, and μ_{wi} is fluid viscosity.

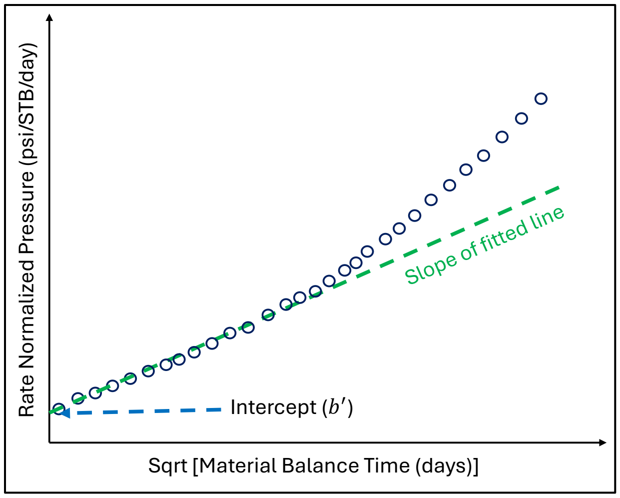

Figure 3: Square-root-of-time RTA plot showing the straight-line fit during the linear flow regime. The intercept obtained from the fitted line is used to calculate skin and the dimensionless fracture conductivity

The estimated intercept (b') was then used to compute the dimensionless apparent fracture conductivity (Fcd'), from the analytical relationship (Clarkson, 2021):

$$Fcd' = \frac{141.2 B_o \mu_o}{b' k h n_f}\left(1 + \frac{h}{x_f}\left[ln\left\{\frac{h}{2r_w}\right\} - \frac{\pi}{2}\right]\right) \tag{6}$$

An equivalent formulation relating fracture skin to fracture conductivity is also commonly used:

$$Fcd' = \frac{1}{s} \cdot \frac{2x_f}{h}\left(1 + \frac{h}{x_f}\left[ln\left\{\frac{h}{2r_w}\right\} - \frac{\pi}{2}\right]\right) \tag{7}$$

These analytical relationships allow estimation of apparent dimensionless fracture conductivity directly from the intercept of the square-root-of-time RTA plot. The calculated F_{cd}' provides a measure of fracture effectiveness by comparing fracture flow capacity relative to reservoir flow capacity.

Clarification on the interpretation of calculated LFP:

- Absolute-Permeability LFP: this is the linear flow parameter calculated using absolute permeability as below:

$$LFP_{abs} = A_f\sqrt{k_{abs}} \tag{8}$$

- Effective-Permeability LFP for individual phases: this is the linear flow parameter calculated using effective permeability. For oil and water phase, it is calculated as below:

$$LFP_o = A_f\sqrt{k_{abs}k_{ro}} \tag{9}$$

$$LFP_w = A_f\sqrt{k_{abs}k_{rw}} \tag{10}$$

- Total-fluid LFP (LFP_{ow}): when performing total-fluid RTA, the overall LFP obtained is related to the individual phase LFP as below (Appendix A):

$$LFP_{ow} = \sqrt{{LFP_o}^2 + {LFP_w}^2} \tag{11}$$

Pseudopressure formulation and estimation

Pseudopressure was originally introduced by Al-Hussainy et al. (1966) to account for the nonlinear effects of pressure-dependent properties, providing a convenient transformation that linearizes the flow equation. Building on this framework, Raghavan (1976) proposed modifications to the pseudopressure definition to incorporate relative permeability effects. Subsequent studies extended these formulations to a wider range of flow regimes and conditions, for example, Behmanesh et al. (2015) presented adaptations applicable to linear flow analysis. Because pseudopressure transformations already capture pressure-dependent variations in properties such as viscosity and permeability, they can be naturally extended to include relative permeability effects within the same unified framework. The pseudopressure formulation used in this paper is illustrated Equation (12).

$$P_{po}(p) = \left(\frac{B_o\mu_o}{k}\right)_i \int_0^p \frac{k_{ro}(p)k(p)}{B_o(p)\mu_o(p)} dp \tag{12}$$

Here, p – pressure, $P_{po}(p)$ – pseudopressure as a function of pressure, $k_{ro}(p)$ – relative permeability as a function of pressure, $k(p)$ – permeability as a function of pressure, $B_o(p)$ – oil formation volume factor as a function of pressure, $\mu_o(p)$ – oil viscosity as a function of pressure, $subscript -\ i$ means initial values.

Simulation approach

Simulations were performed with the integrated hydraulic fracturing and reservoir simulator described by McClure et al. (2025). The simulations combine flow in the well, hydraulic fractures, and the reservoir. In each timestep, governing and constitutive equations are solved in each type of element: (a) flow and momentum balance in the well, (b) flow, proppant transport, and fracture mechanics in the fractures, and (c) flow and poro-elasticity in the matrix. The simulations include fracturing, shut-in, flowback, and potential long-term production in a single continuous simulation.

The simulation setup and results can be compared directly with the values estimated from RTA. For example, LFP_o is calculated by taking the summation of area times the square root of k_o for every matrix-fracture element flow connection that is assigned to a fracture element that is counted as 'propped' (containing more than an average of 0.01 lbs/ft^2 of proppant).

Original oil/gas/water in place is calculated by: (a) visually estimating the drained fracture length from the simulation results by inspecting the length of the depleted pressure region along the hydraulic fractures, (b) multiplying drained fracture length by lateral length to calculate drained area, and (c) multiplying drained area by production per areal extent, which is calculated by summing the fluid in place across the stratigraphic column of the depth intervals that are being produced from.

Summary of the simulations

Synthetic simulation examples and field datasets were analyzed in this study. Several simulations were conducted, including both single-phase water and multiphase flow cases. The base case synthetic model represents a generic North American unconventional reservoir well with a matrix permeability of 50 nD and utilizing multistage hydraulic fracturing. This base case serves as the reference scenario against which all sensitivity simulations are compared. The basic parameters of the base case simulation are summarized in Table 1.

Table 1: Basic input parameters for the base case single-phase synthetic simulation

Parameter	*Value*
Reservoir permeability, nD	50
Porosity, %	5

Initial reservoir pressure, psi	6650
Fluid system	Single-phase water
Number of fractures	8
Fracture spacing, ft	25
Fluid viscosity, cP	0.3262
Fluid FVP, rbbl/STB	1.01

Utilizing the base case as the reference scenario, several additional simulations were conducted to investigate increasing levels of reservoir and fracture complexity. These include cases representing multiphase flow, bounded reservoirs, fractal fracture networks, pressure-dependent permeability, stimulated reservoir volume (SRV) effects, and fracture conductivity loss with both drawdown and time. Each simulation case and its corresponding definition are summarized in Table 2.

Table 2: Summary of synthetic simulation cases used in this study

Simulation	*Description*
SP	Base case single-phase water
SP-PDP	Single-phase water with pressure-dependent permeability loss with drawdown
SP-ZPC	Single-phase water with zero-permeability cube to simulate the effect of production interference from neighboring wells
SP-TDC	Single-phase water with time-dependent conductivity loss – TDC (Section 19.7 from McClure et al., 2025)
SP-FS	Single-phase water with fractal fracture swarms (Section 19.11 from McClure et al., 2025)
SP-SRV	Single-phase water with an assumed 'SRV' of elevated permeability in the area surrounding the hydraulic fracture
MP	Multiphase base case with oil, water and gas
MP-PDP	Multiphase case with pressure-dependent permeability loss with drawdown
MP-ZPC	Multiphase case with zero-permeability cube to simulate the effect of production interference from neighboring wells
MP-TDC	Multiphase case with time-dependent conductivity (Section 19.7 from McClure et al., 2025)
MP-FS	Multiphase case with fractal fracture swarms (Section 19.11 from McClure et al., 2025)
MP-SRV	Multiphase case with an assumed 'SRV' of elevated permeability in the area surrounding the hydraulic fracture
MP-PDP+ZPC	Multiphase case with pressure-dependent permeability and zero-permeability cube
MP-PDP+ZPC+TDC	Multiphase case with pressure-dependent permeability & zero-permeability cube, and time-dependent conductivity loss
MP-TDC+ZPC	Multiphase case with time-dependent conductivity loss and zero-permeability cube

In addition to the synthetic simulation cases described above, several field datasets and corresponding history-matched simulations were analyzed in this study. A total of five field datasets were used, including four wells from the Bakken formation (BK1, BK2, BK3, and BK4) and one well from the Permian Basin (PM1).

The BK1 dataset is from the Bakken formation and consists of a production well drilled in the Middle Bakken. One pressure-monitoring well is located in the Middle Bakken, while another monitoring well is placed in the underlying Three Forks formation. Both monitoring wells are cased, cemented, and were never perforated. They are equipped with cemented fiber-optic cables and arrays of external casing pressure gauges that record formation pressure during hydraulic stimulation as well as during long-term production. Details of the well configuration and monitoring system are provided in previous studies (Liang et al. 2022; Singh et al. 2025). For the other datasets, the model setup, geological properties, and completion design for these wells are described in detail in Singh et al. (2025) and Morsy et al. (2025). The BK2 well is described in detail by Cipolla et al. (2022). In the present study, the previously calibrated field models were used to evaluate the diagnostic behavior of the rate transient analysis workflows described above.

Results

Testing the accuracy and robustness of common RTA techniques

Early deviation from linear flow

Figure 4 shows Square-Root-of-Time RTA plot of the single-phase with PDP (pressure dependent permeability loss) simulation. Curves are provided both with and without a pseudopressure adjustment (pseudotime adjustment was not used). Without pseudopressure adjustment, the data shows an almost immediate deviation from linearity. For practical purposes, an interpreter may not be certain whether or not PDP is present. Should the test be interpreted as indicating an early deviation from linear flow due to fracture-to-fracture interference, due to pressure-dependent permeability loss, or something else?

If Equation (2) is used to estimate permeability from this data, then the result is 288 nD without pseudopressure correction and 68 nD with pseudopressure correction. The large discrepancy occurs because without pseudopressure correction, the early deviation from linear flow may be interpreted as fracture-to-fracture interference, which would imply very high diffusivity and therefore a high permeability. The 'true' base permeability used in the simulation was 50 nD, and with depletion, the system permeability decreased further.

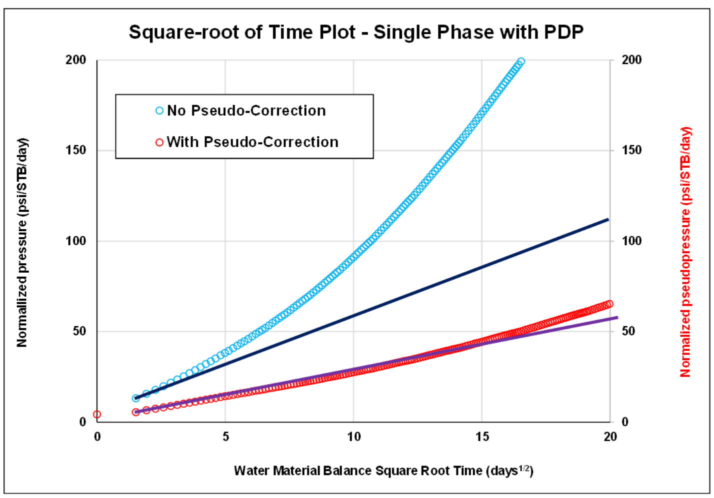

Figure 4: Comparison of the Square-Root-of-Time RTA plot with and without pseudocorrection in the SP-PDP simulation.

In a practical case, how might we assess whether to interpret that: (a) the formation has high permeability/early interference, or (b) that it is losing productivity due to PDP loss, multiphase flow, or another process?

The best approach for collapsing nonuniquness is to synthesize field diagnostics. For example, diagnostic fracture injection tests (DFITs) provide in-situ permeability estimates (McClure et al., 2020; 2024). Interference tests can be used to constrain propped length (Almasoodi et al., 2023; Ponners et al., 2024; Singh et al., 2025); geochemical analysis can be used to estimate depleting height (Bachleda et al., 2024), and downhole imaging and cross-well fiber can be used to estimate fracture spacing (Ugueto et al., 2023; Bourgeois et al., 2026). All of these measurements combined, plus production history matching with RTA and/or numerical simulation, can constrain the key reservoir parameters.

In some cases, independent measurements such as core may be available. For example, Jongeling et al. (2024) describes an integrated modeling study in the Marcellus, where core measurements were used to estimate the magnitude of PDP loss, and these values were integrated into field-scale model calibration.

In the absence of comprehensive diagnostics, the interpreter may rely on play-specific knowledge. For example, it is generally recognized that the highly overpressured Haynesville experiences pressure-dependent permeability loss. Also, as discussed in the diagnostic trend section, RTA and GOR trends can be analyzed to diagnose different physical processes.

The consequences of misidentifying formation processes can be important. Fowler et al. (2019) reviewed a Utica shale dataset where it was possible to perform a production history match with different permeability values, varying over orders of magnitude. A match utilizing higher permeability could compensate by assuming shorter productive half-length. Remarkably, even after 30 years, the models assuming drastically different permeabilities and effective fracture lengths yielded similar production predictions. However, if the differing models were used to optimize well spacing and cluster spacing, they yielded drastically different recommendations.

To summarize, while pseudopressure adjustment can be used to account for nonlinearity in RTA analysis, this cannot be performed in isolation. Contextual reservoir information and field diagnostics are critical for identifying when and how to use pseudopressure and numerical RTA adjustments.

Assessing the impact of pseudopressure assumptions

Figure 5 and Figure 6 show crossplots of ‘actual’ versus ‘RTA-estimated’ LFP and OFIP for all the simulations considered in this study (summarized in the Method section), analyzed with and without pseudopressure adjustment. The pseudopressure adjustments were performed with ‘known’ values for relative permeability, PDP, and initial fluid saturations.

Because the pseudopressure adjustments were performed with knowledge of the correct adjustment, the fluid-in-place and LFP estimates were accurate across the range of results. Without adjustment, the LFP and OFIP values tended to be underestimated, with up to 100-200% error. This occurred because changes in fluid viscosity and compressibility with pressure distort the pressure-flow relationship, causing the slope and intercept used in RTA to shift and leading to underestimation of LFP and OFIP.

The permeability estimates without adjustment were notably inaccurate, particularly using Method 1 (Equation 2). Method 1 assumes that deviation from linear flow occurs because of fracture-to-fracture interference; if instead, the deviation occurs because of another source of nonlinearity (multiphase flow, pressure dependent permeability loss, etc.), then it will overestimate permeability. In theory, with perfect pseudopressure correction, Method 1 could yield an accurate permeability estimate; however, in practice, the correction cannot be performed with high precision, and so the method is unreliable. Method 2 is somewhat less vulnerable to the effects of nonlinearities and so yields a more reliable estimate. However, as noted earlier, this method requires the system to be in boundary-dominated flow before it can be applied and cannot be used with confidence at early times; moreover, production noise, lift changes, and skin development can significantly complicate OFIP interpretation at late times.

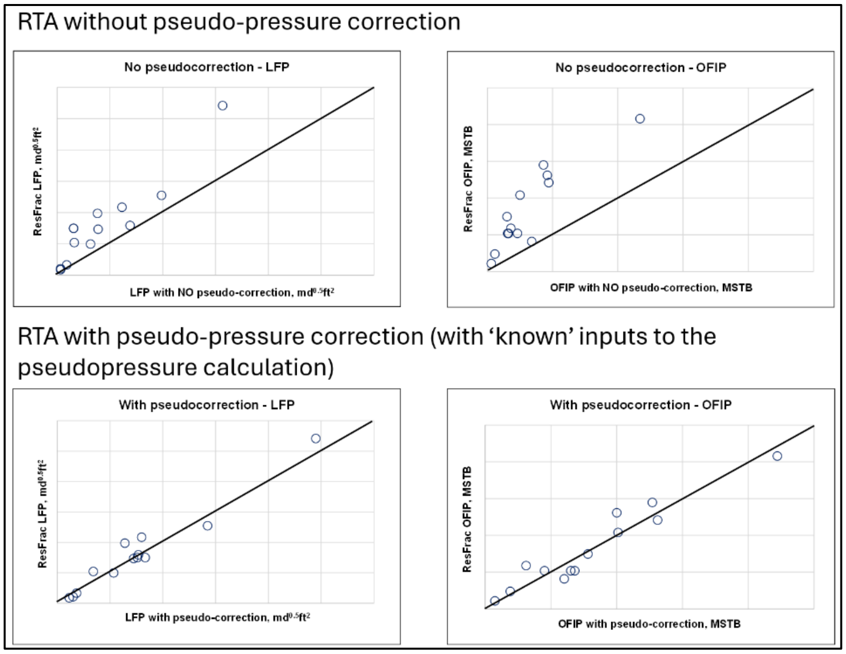

Figure 5: Actual and RTA-estimated effective LFP and OFIP across all simulations with and without pseudopressure correction.

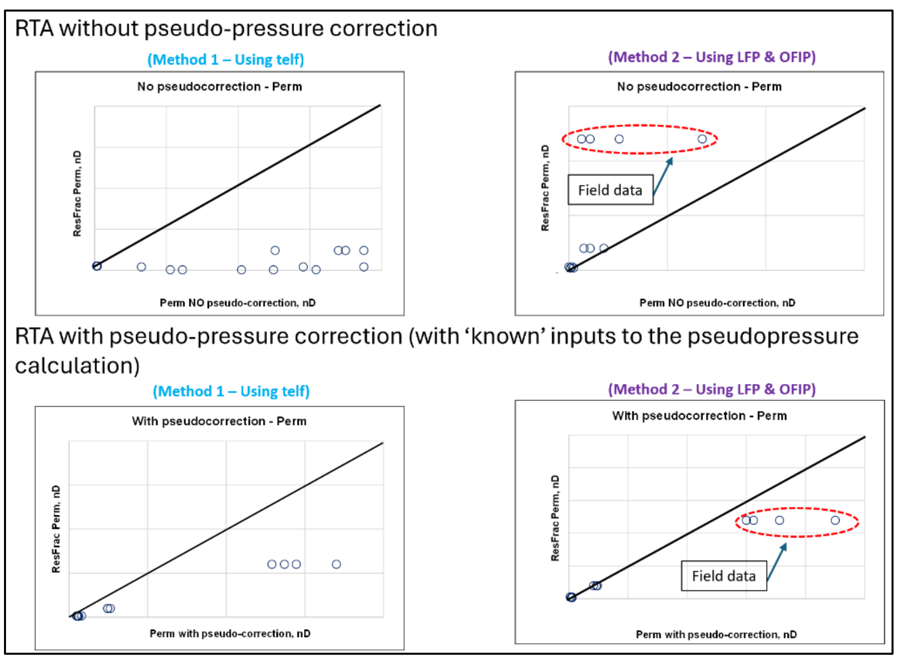

Figure 6: Actual and RTA-estimated permeability across all simulations with and without pseudopressure correction.

Figure 7 shows actual and RTA-estimated LFP and OFIP in the simulations utilizing PDP, where the pseudopressure was calculated assuming 25% higher or lower error compared with actual. Despite the imprecision, the results remained reasonably accurate.

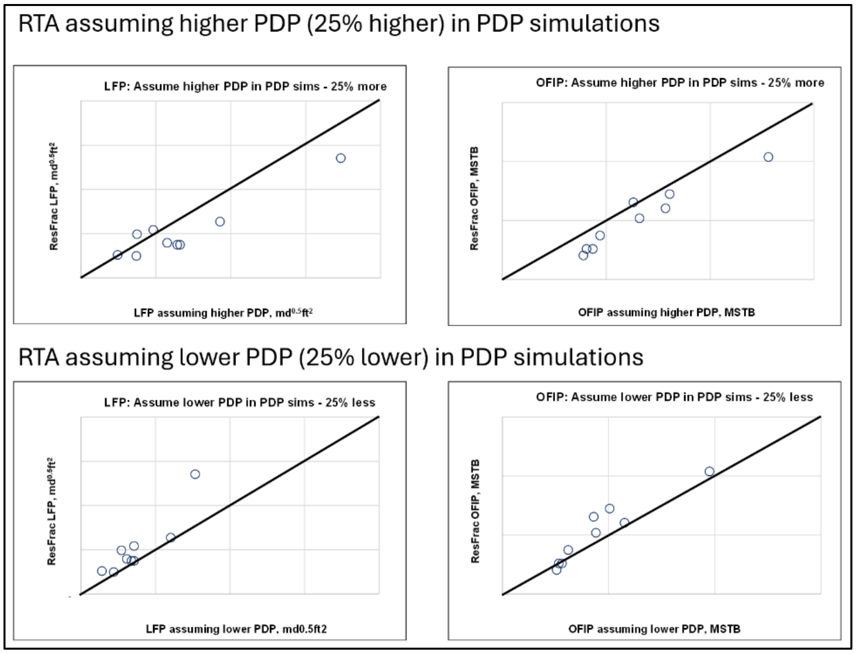

Figure 7: Actual and RTA-estimated effective LFP and OFIP in simulations with PDP, using with pseudopressure corrections assuming 25% more or less PDP than actual.

The LFP and fluid in-place estimates appear to be fairly robust to errors caused by nonlinearities. The LFP is estimated from the early-time slope of the Square Root of Time plot. As shown in Figure 4, nonlinear processes such as multiphase flow and PDP cause productivity loss *after* the slope has been established for LFP estimation. As shown in Figure 2, the fluid in place estimate is made once the fractures have interfered and entered boundary dominated flow, *after* the effect of nonlinearities have had their effect. However, these nonlinear processes can still influence both estimates by altering the effective productivity and pressure response over time, which introduces moderate errors in LFP and OFIP that can reach factors of 2–3 in some cases.

The ‘Method 1’ permeability estimate is vulnerable to nonlinearities, because it depends on identifying the end of linear flow. The ‘Method 2’ permeability estimate is more robust because it effectively integrates the results from the LFP and OFIP approaches, once the well reaches a boundary dominated flow.

RTA using ‘total fluid’ versus using the ‘primary hydrocarbon phase’

RTA analysis can be performed on either ‘total fluid’ or a single phase (either water, oil, or gas, depending on the reservoir). Which is preferable?

The productive hydrocarbon phase (either oil or gas) is what matters economically, and so for this reason, it is often advantageous to estimate LFP and fluid in place with respect to the primary hydrocarbon phase.

However, flowback after fracturing has potential to impact the shape of the diagnostic plot for the primary hydrocarbon phase. Figure 8 shows the simulated production behavior for the multiphase base case (Simulation MP in Table 2), where oil rate declines while GOR and water cut increase over time because of multiphase flow effects. Figure 9 shows the corresponding log-log derivative plots without pseudopressure correction. The left panel of Figure 9 shows the log-log derivative plot of the oil phase. The plot does not exhibit a linear flow period because frac fluid flowback meaningfully distorts the plot during the first several months. If this data was analyzed in isolation without pseudopressure adjustment, it could be ambiguous how to estimate LFP because of uncertainty in where to draw the line. Alternatively, the right panel of Figure 9 shows an RTA log-log derivative plot using total fluid, water plus oil. In this case, the linear flow period is clearly apparent and the plot takes on a much more ideal character.

Figure 10 presents the same simulation with pseudopressure correction applied. In this case, both the hydrocarbon-phase and total-fluid plots show clear linear-flow regimes, and LFP can be estimated accurately. These comparisons show that although pseudopressure correction is needed to properly account for multiphase effects, total-fluid RTA without pseudopressure correction may still provide a reliable estimate of flow regime and LFP in some cases (for oil/water systems; we did not evaluate the total fluids approach for gas/water systems in this study). This is most likely when the effective compressibility behavior of the flowing oil-water system is sufficiently similar between phases.

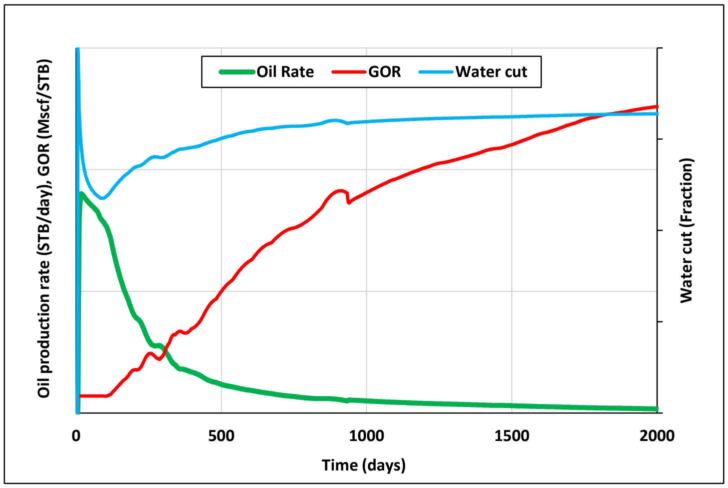

Figure 8: Oil production rate, gas–oil ratio (GOR), and water cut versus time for the multiphase (MP) simulation case.

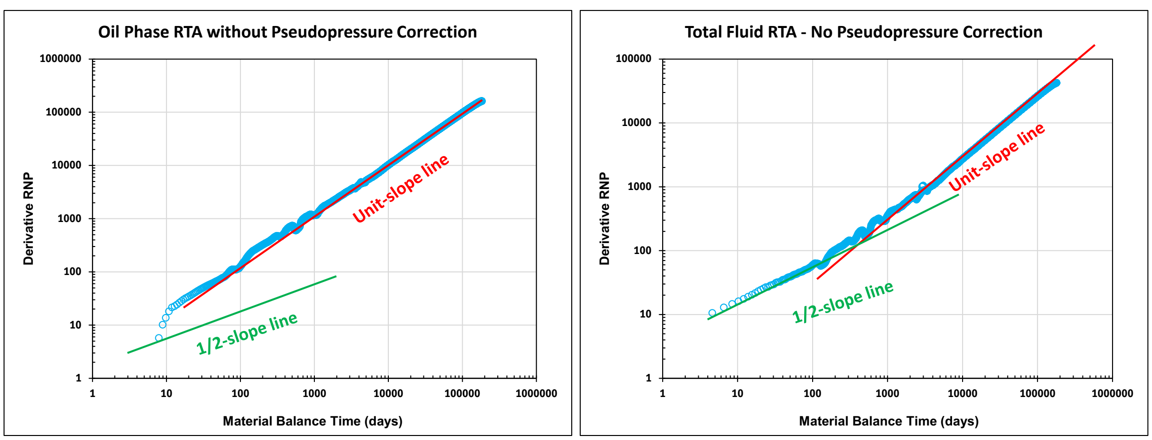

Figure 9: RTA plot of the results from Simulation MP without pseudopressure adjustment. The left panel shows an analysis solely of the oil data. The right panel shows an analysis of the oil (at reservoir conditions) plus water.

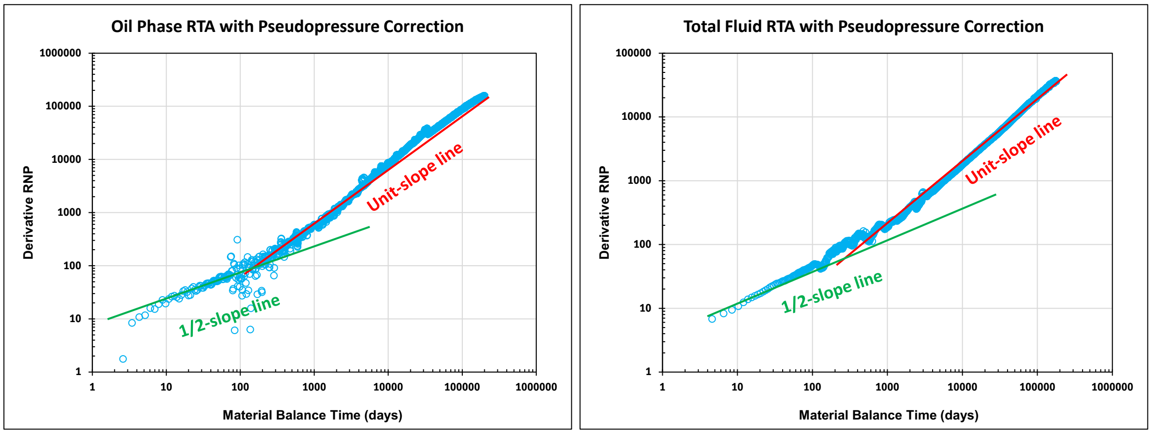

Figure 10: RTA log-log derivative plot of the results from Simulation MP with pseudopressure adjustment. The left panel shows an analysis solely of the oil data. The right panel shows an analysis of the oil (at reservoir conditions) plus water.

In practice, real datasets will not always look like Figure 9. Very often, a linear flow period develops cleanly on an RTA plot using the primary hydrocarbon phase and adjusting for pseudopressure as illustrated in Figure 10. This is evidently because water leakoff and flowback are not sufficiently blocking the beginning of hydrocarbon production.

Nevertheless, if the diagnostic plots using the hydrocarbon phase does not show a clean linear flow period, then it can be very helpful to make a plot using total fluid. In this case, if LFP is estimated from the oil/water or gas/water data, it will be desirable to convert this to LFP_o or LFP_g, the LFP solely for the hydrocarbon phase (Appendix A).

There is no universal water-cut threshold for selecting between hydrocarbon-phase and Total-Fluid RTA. In practice, the choice is governed by flow stability rather than a fixed water cutoff. When early-time production is dominated by frac-fluid cleanup, typically reflected by high and rapidly evolving water cut, GOR, and rates, hydrocarbon-phase RTA may not exhibit a reliable linear flow regime, and Total-Fluid RTA is generally preferred. As production stabilizes and these parameters begin to follow consistent trends representative of reservoir flow, hydrocarbon-phase RTA becomes increasingly reliable for interpretation.

Effect of conductivity

Recent projects utilizing far-field pressure monitoring wells have shown that proppant packs in shale exhibit 1000s of psi of pressure gradient along their length (Singh et al., 2025). How do these observations relate to RTA and production? Does proppant pack conductivity matter for production?

Singh et al. (2025) matched numerical models to the datasets from Liang et al. (2022) and Cipolla et al. (2022). The estimated values of proppant pack conductivity were 3-8 md-ft. The implied values of dimensionless fracture conductivity were 3.8 and 8.7 for the two datasets. These two datasets correspond to the BK1 and BK2 models used in this study. Figure 12 from Liang et al. (2022) shows the setup of the wells for the BK1 dataset.

Considering these observations, do we see evidence of finite conductivity in the RTA trends? The left panel of Figure 11 shows the square root of time plot from the well from Liang et al. (2022). Surprisingly, a y-intercept is not clearly apparent. The right panel of Figure 11 shows the square root of time plot of the numerical model history match to the data. The presence of a y-intercept is debatable, depending on where the straight line is drawn.

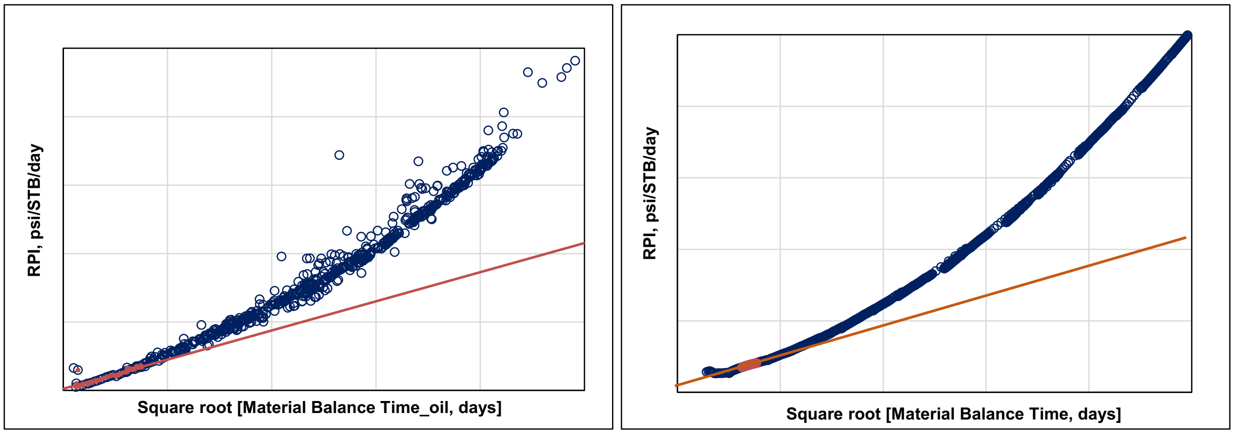

Figure 11: Rate-transient trend from the Well P1 from Liang et al. (2022).

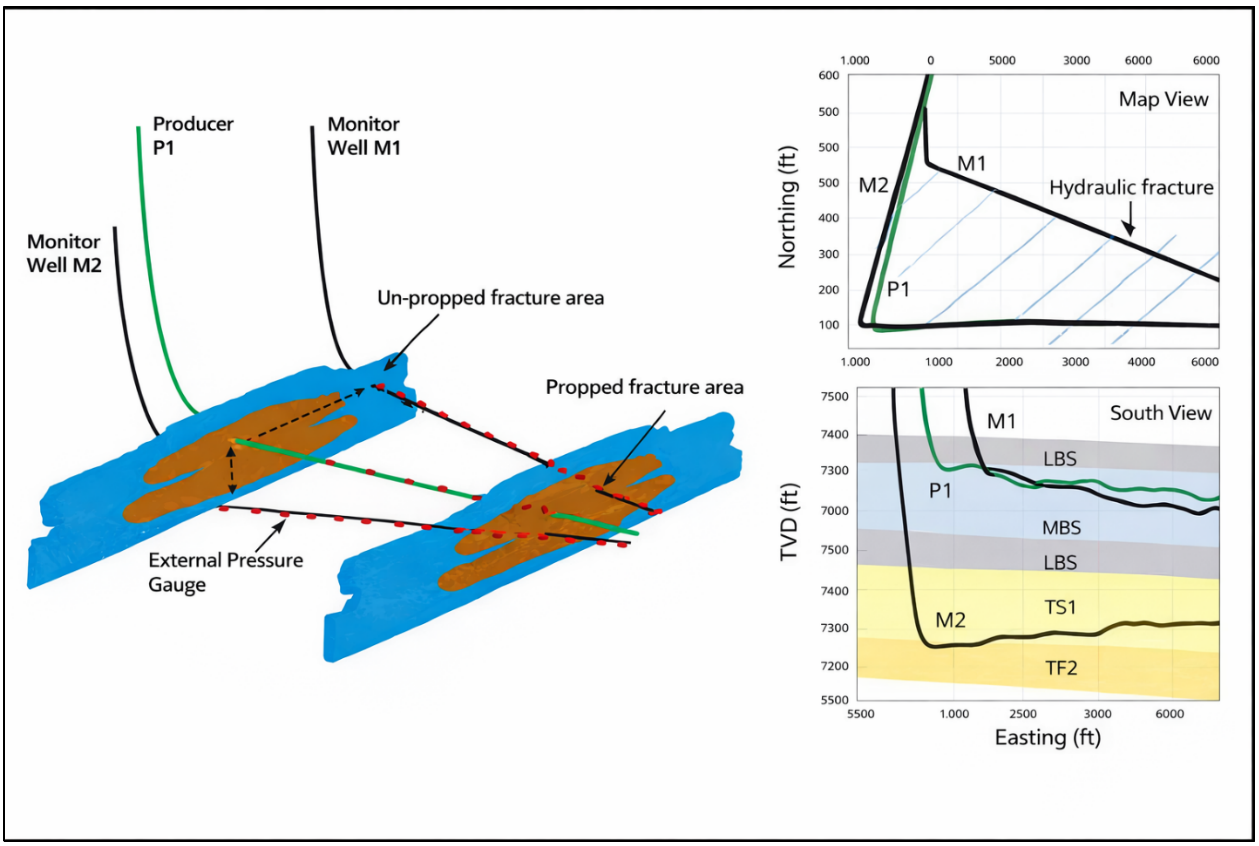

Figure 12: Fracture geometry from the simulation of the BK1 Liang et al. (2022) dataset, reproduced from Liang et al. (2022).

Even with fairly low dimensionless fracture conductivity, the y-intercept in the square root of time plot is small and hard to see in these cases. One problem is that the y-intercept is highly dependent on the assumption of initial reservoir pressure. However, reservoir pressure is elevated in the vicinity of the fracture following fracturing and fracture closure. As a result, the 'initial reservoir pressure' is not clearly defined for early time, and this ambiguity can swamp any apparent y-intercept, unless it is very large.

Conductivity estimates from far-field pressure observation wells and from interference tests suggest that fracture conductivity starts in the range of double-digit md-ft, and decreases to single-digit or lower with time and drawdown (Singh et al., 2025). Based on our studied field cases, this result is concordant with observations from RTA because fractures can be finite conductivity *even though* there is usually not a clearly apparent y-intercept on the square root of time plot.

We reran the BK1 simulation with a 2x increase in conductivity. The result was a 16% increase in production after 1 year. This shows that, depending on conditions, proppant pack conductivity *does* matter for production, even though maximizing LFP remains the most important consideration for fracture design.

Figure 13 shows production versus time for our base case simulation, Simulation SP, with conductivity varied upwards and downwards by a factor of 100x. Figure 14 shows the pressure distribution inside the fractures for the base case and low conductivity case.

As would be expected from classical theory, the effect of conductivity on production depends on the dimensionless fracture conductivity, Fcd'. As noted by Almasoodi et al., (2023), the classical definition of dimensionless fracture conductivity is technically only valid for radial flow, and an alternative 'linear flow' definition can be used instead. Nevertheless, for convenience and familiarity, we calculated Fcd' using the standard definition.

For values of Fcd' exceeding 100, conductivity had little impact, and there was little apparent pressure gradient in the proppant pack. However, with dimensionless conductivity of single or double digits – values realistic for slickwater fracturing in shale – then increasing conductivity had a meaningful impact on production.

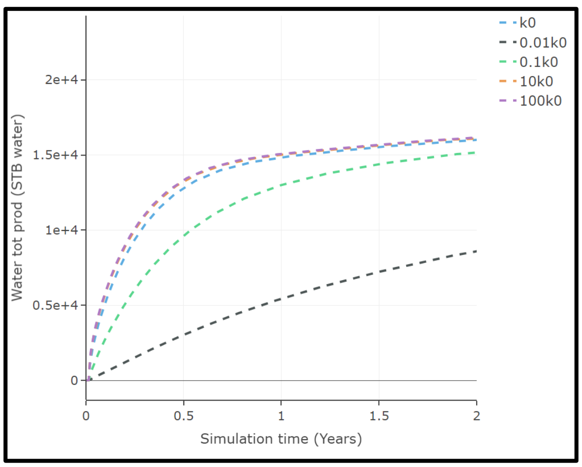

Case study	Permeability, nD	Fracture Conductivity @ 1-year, mD-ft	Skin	FcD
Case 1 - 0.01x	50	0.39	0.468	2
Case 2 - 0.1x	50	2.9	0.053	22
Case 3 – 1x	50	26	-0.005	224
Case 4 – 10x	50	254	-0.011	2225
Case 5 – 100x	50	2536	-0.012	22159

Figure 13: Production versus time for Simulation SP, varying fracture conductivity upwards and downwards by a factor of 100x.

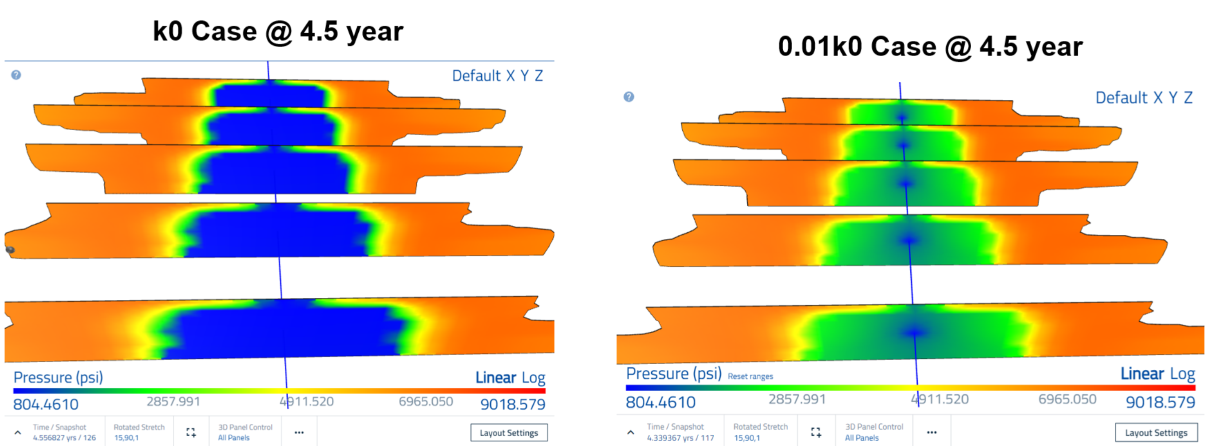

Figure 14: Pressure distribution at 4.5 years in the base Simulation SP (left) and with proppant pack conductivity reduced by 100x (right).

Diagnosing reservoir behaviors from RTA and GOR trends

Diagnostic trends

When performing RTA or numerical modeling, it is necessary to evaluate assumptions about key physical processes, in order to know what physics to include in the calculations. For this purpose, Figure 15, Figure 16, and Figure 17 show schematics of the derivative plot of RPI (Reciprocal of Productivity Index) and GOR trends that result from different sources of non-ideality. These figures are based on the results from the simulations run in this study. They are intended to be used qualitatively, and they provide guidelines, not absolute rules. Interpretations should be performed by taking into account the full context of a dataset. For example, GOR increases are usually larger with higher GOR fluids, a phenomenon that affects the magnitudes of the trends shown in Figure 16.

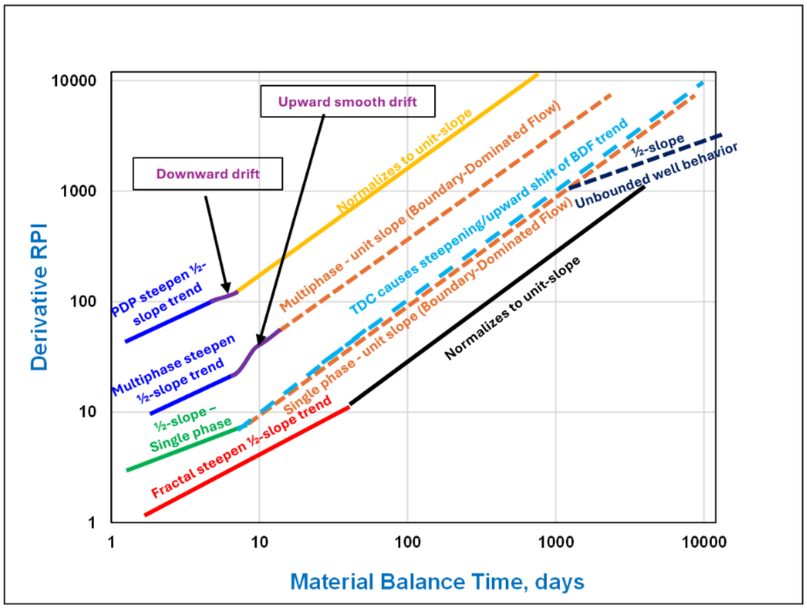

Figure 15: Schematic showing the log-log derivative RTA plot response caused by different sources of nonideality. These plots are intended to be used with unconventional shale wells.

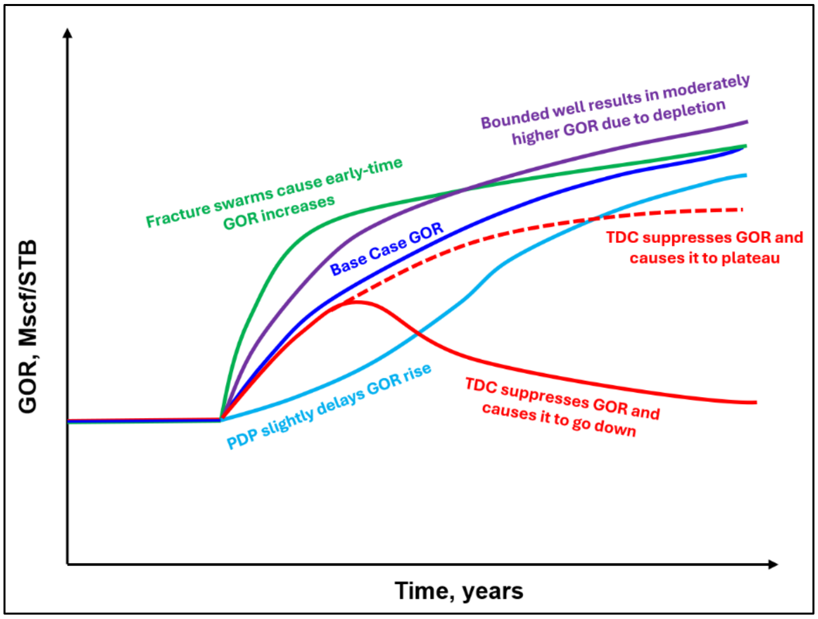

Figure 16: Schematic showing the GOR trend resulting from different sources of nonideality. These plots are intended to be used with unconventional shale wells. In addition to what is shown on the figure, the GOR response also depends strongly on fluid properties, with higher GOR fluids tending to show greater GOR increase after dropping below the saturation pressure.

Physical Mechanism	Simple single/multiphase baseline behavior	Simple baseline – bounded/unbounded	Pressure-dependent permeability (PDP)
Signature on loglog RPI Derivative Plot	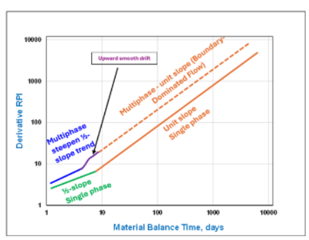	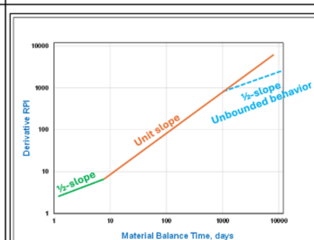	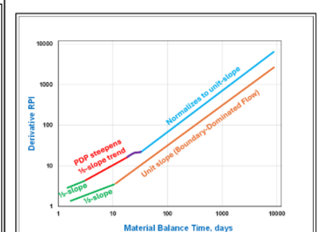
Signature on GOR Plot	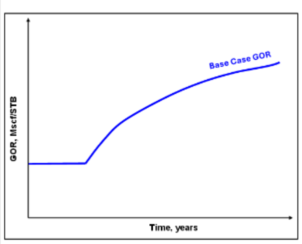	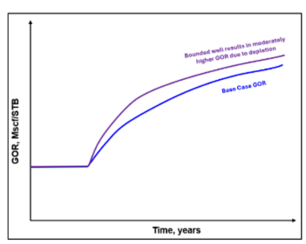	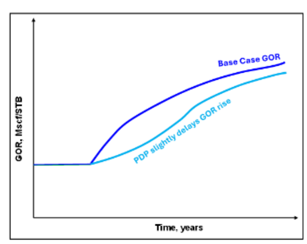

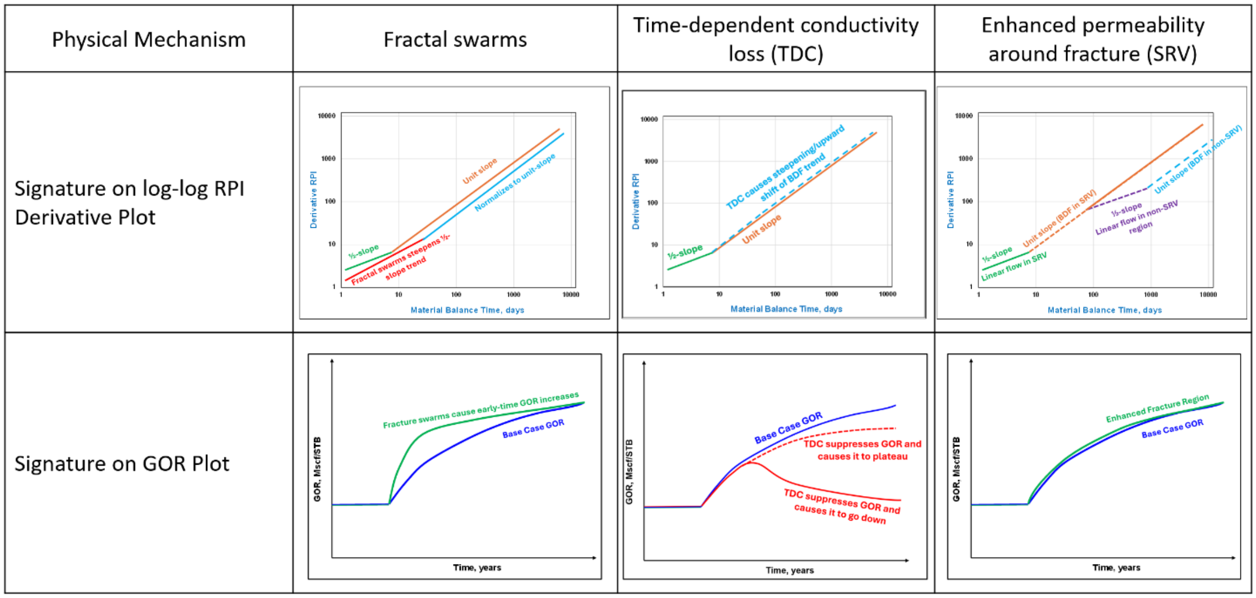

Figure 17: Schematic showing the RTA and GOR responses caused by different sources of nonideality. These plots are intended to be used with unconventional shale wells.

To summarize the trends:

1. The baseline behavior of an unconventional shale well is to experience linear flow (1/2 slope) followed by a transition to boundary-dominated flow (1 slope). If the well is unbounded, it is theoretically possible that there could be a later transition into a second linear flow period corresponding to flow in the direction along fracture strike (instead of perpendicular to the fractures). This behavior is also supported by tri-linear flow models, which describe sequential flow from the reservoir to the fracture and along the fracture, including late-time linear flow parallel to fracture strike (e.g., Barzin and Mattar 2017, Ozkan et al., 2011 and Brown et al., 2011). However, most wells are bounded, and a late-time linear flow period is prevented by production interference. Holding everything else equal, bounded wells will experience somewhat greater GOR increase than unbounded wells.

2. In multiphase systems, the early-time linear flow (1/2 slope) often steepens due to changing fluid mobility and saturations. The transition period is characterized by an upward shift in the response, rather than a clean linear transition. At late time, the system reaches boundary-dominated flow (unit slope).

3. With pressure-dependent loss of system permeability with drawdown, the onset of PDP will tend to steepen the slope of the derivative log-log plot above 1/2. This might be followed by a direct transition into boundary dominated flow. However, in some cases, we observe a subsequent period of *flattening* after the steepening, but before reaching the 1.0 slope of the boundary dominated period. PDP loss tends to delay and weaken the GOR rise, because it reduces the rate that pressure can be drawn down in the system surrounding the fractures.

4. Time-dependent conductivity loss (TDC) occurs gradually over the course of years, and may continue to worsen indefinitely (Pearson et al., 2023). It is a distinct from conductivity loss due to pressure drawdown, which typically occurs in the first 6-24 months of production. Very strong TDC can cause GOR to reach a maximum and subsequently decrease. While this is apparent in some field datasets, this is not typical. Mild-to-moderate TDC suppresses GOR increase in the long-term but is not strong enough to cause a reduction. On the log-log plot, TDC stretches the

boundary dominated flow period by extending the apparent material balance time duration of the transient. It can also slightly translate the square root of time curve upwards during the boundary dominated flow period and/or cause a slight steepening.

5. Fractal fracture swarms have been hypothesized by Acuña, (2020) to be the cause of non-ideal RTA behavior. The phenomenon causes the log-log plot to immediately start at a slope greater than 1/2 – with no true 'linear flow' period ever observed. Although – as noted in Section 3.2 – water flowback at early time can obscure the linear flow period if the data is plotted with respect to the primary hydrocarbon phase. Plotting total fluids may cause a linear flow period to become apparent. Thus, attention must be paid to not mistake flowback/multiphase flow effects for fractal swarms. In simulations, fractal swarms cause GOR to rise rapidly because of the strong pressure drawdown in the rock between closely spaced fractures.
6. It is sometimes hypothesized that hydraulic fractures are surrounded by an "SRV" region of elevated permeability. If this occurs, it can cause an early "apparent" boundary dominated flow, as the radius of investigation reaches the edges of the SRV region. There might be a subsequent linear flow period after fluid begins to flow inwards from the surrounding non-SRV rock

In the authors' experience performing numerical modeling and RTA workflows, we usually do not utilize mechanisms #5 and #6 – fractal fracture swarms and SRV. We do sometimes observe RTA log-log derivative plots that exhibit an early deviation from linear flow. However, this is not usually accompanied by a corresponding large rise in GOR. Also, we do not typically see a 'second' linear flow period, which could be a consequence of an SRV region with enhanced permeability around the hydraulic fractures.

Published core-through studies do not report evidence of SRV-like permeability enhancement regions around hydraulic fractures (Raterman et al., 2020). Core-through studies do suggest that there are a large number of hydraulic fracture strands, forming 'swarms.' This observation does appear to support the fractal fracture swarm concept. However, observations also suggest that most hydraulic fracture strands are likely unpropped and so while they contribute to leakoff during fracturing, they may make a limited contribution to production (Raterman et al., 2020).

Field example

This section steps through an example of how the results from the section above can be used to diagnose reservoir processes from practical data. Figure 18 shows the RTA and GOR trends from the field dataset that was the basis for Simulation BK1. As BHP decreases below the saturation pressure, the GOR increase is mild. The data exhibits a linear flow period, followed by a gradual steepening and transition to a unit slope.

Because of the relatively muted GOR increase, we should not favor the interpretations that either: (a) there are large decreases in oil relative permeability below the bubble point, or (b) that there are fractal fracture swarms. Instead, the data favors an interpretation that there are mild relative permeability effects. Based on the results in the section above, some degree of pressure-dependent permeability loss and/or time-dependent fracture conductivity loss could be considered in the match. In fact, these processes were both included in the calibrated history match performed on this dataset by Singh et al. (2025), which utilized a variety of other data sources for constraining and calibration, including far-field pressure observations.

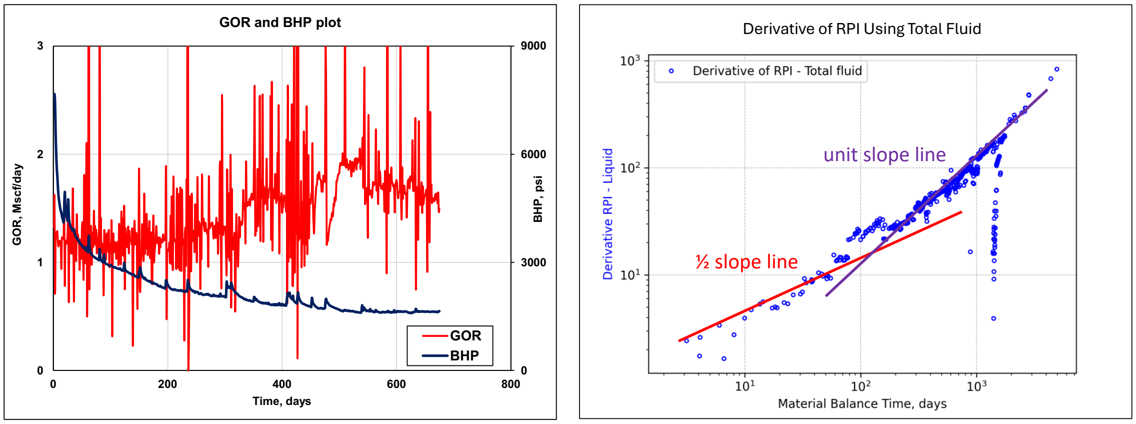

Figure 18: GOR and RTA trends from the field data that was the basis for Simulation BK1.

Conclusions

Primary conclusions from this study are:

1. With appropriate pseudopressure and/or numerical RTA adjustments, it is theoretically possible to yield accurate parameter estimates across a range of nonlinear conditions. However, accuracy depends on good assumptions regarding nonlinear effects. LFP and fluid in place estimates are more robust to error than permeability estimates. The method of estimating permeability based on the time to deviation from linear flow is particularly unreliable.
2. In some datasets, the linear flow period is obscured by flowback if the data is plotted solely with respect to the primary hydrocarbon phase. In these cases, it may be advantageous to calculate the total reservoir flow rate and replot the data. If an LFP estimate is made from the total flow rate, it is possible to back-calculate the LFP with respect to the hydrocarbon phase.
3. Finite proppant pack conductivity has been documented in recent studies utilizing pressure observation laterals. Our results show that if we use realistic, fairly low values for proppant pack conductivity, it is in some cases still difficult to discern a y-intercept on the square root of time plot. These results demonstrate that there is no inconsistency between reported far-field pressure observations and RTA.
4. Summarizing results from a variety of simulations, we created plots with schematics of RTA and GOR trends that correspond to different flow regimes and physical phenomena. These plots can be used to guide diagnosis of physical processes in RTA and numerical modeling workflows.

Acknowledgements

We gratefully acknowledge the support of APA Corporation, ConocoPhillips Company, Continental Resources, Devon Energy, ExxonMobil Corporation, Hess Corporation, and Chevron U.S.A. Inc. Thank you to our colleagues who provided helpful feedback on the manuscript.

Nomenclature

$\boldsymbol{A_f}$ – fracture area, ft^2

$B_o(p)$ – oil formation volume factor as a function of pressure, rbbl/STB

$\boldsymbol{B_{wi}}$ – water formation volume factor, rbbl/STB

$\boldsymbol{b'}$ – intercept of the Square-Root-of-Time plot, psi/STB/day

$\boldsymbol{c_t}$ – total effective compressibility, 1/psi

$F_{cd}{}'$ – dimensionless fracture conductivity

h – reservoir thickness, ft

k – permeability, md

$k(p)$ – permeability as a function of pressure, md

$k_{ro}(p)$ – relative permeability as a function of pressure

LFP_{abs} – absolute-permeability LFP, $ft^2md^{0.5}$

LFP_o – effective oil LFP, $ft^2md^{0.5}$

LFP_{ow} – total-fluid LFP, $ft^2md^{0.5}$

LFP_w – effective water LFP, $ft^2md^{0.5}$

L_w – effective horizontal length, ft

$\boldsymbol{n_f}$ – number of effective fractures

p – pressure, psi

$P_{po}(p)$ – pseudopressure as a function of pressure, psi

S_{wi} – initial water saturation

s' – skin

t_{elf} – time to end linear flow, days

x_f – fracture half-length, ft

$\mu_o(p)$ – oil viscosity as a function of pressure, cP

$\boldsymbol{\mu_w}$ – water viscosity, cP

$\boldsymbol{\phi}$ – porosity, fraction

References

Acuña, J.A. 2020. Rate transient analysis of fracture swarm fractal networks. Paper URTeC-2020-2118-MS presented at the SPE/AAPG/SEG Unconventional Resources Technology Conference, Virtual, July 2020. doi: 10.15530/urtec-2020-2118.

Agarwal, R.G., Gardner, D.C., Kleinsteiber, S.W., and Fussell, D.D. 1999. Analyzing well production data using combined-type-curve and decline-curve analysis concepts. SPE Reservoir Evaluation & Engineering 2 (5): 478–486. doi: 10.2118/57916-PA.

Al-Hussainy, R., Ramey, H.J. Jr., and Crawford, P.B. 1966. The flow of real gases through porous media. *Journal of Petroleum Technology* 18 (5): 624–636. doi: 10.2118/1243-PA.

Almasoodi, M., Andrews, T., Johnston, C., Singh, A., and McClure, M. 2023. A new method for interpreting well-to-well interference tests and quantifying the magnitude of production impact: Theory and applications in a multi-basin case study. *Geomechanics and Geophysics for Geo-Energy and Geo-Resources* 9 (1): 95. doi: 10.1007/s40948-023-00632-1.

Aziz, K. and Settari, A. 1979. *Petroleum reservoir simulation*. London: Applied Science Publishers.

Bachleda, J., Cisneros, R., Carson, D., Donahue, H., Manigold, M., Jin, M., Ge, S., Wu, J., and Liu, F. 2024. Optimizing infill development in the Delaware Basin through integration of geochemistry, tracer, pre-frac step-down test, and pressure data. Paper URTeC-2024-4042489-MS presented at the SPE/AAPG/SEG Unconventional Resources Technology Conference, Houston, Texas, USA, June 2024. doi: 10.15530/urtec-2024-4042489.

Barzin, Y., and Mattar, L. 2017. Limitations of Current Type Curves in Characterizing SRV; and Development of EFR Type Curves. Paper presented at the SPE Unconventional Resources Conference, Calgary, Alberta, Canada, February 2017. https://doi.org/10.2118/185038-MS

Behmanesh, H., Hamdi, H., and Clarkson, C.R. 2015. Analysis of transient linear flow associated with hydraulically fractured tight oil wells exhibiting multiphase flow. Paper SPE-172928-MS presented at the SPE Middle East Unconventional Resources Conference and Exhibition, Muscat, Oman, 26–28 January 2015. doi: 10.2118/172928-MS.

Blasingame, T.A., and Lee, W.J. 1988. Variable-rate reservoir limits testing of gas wells. Paper SPE-17708-MS presented at the SPE Gas Technology Symposium, Dallas, Texas, USA, June 1988. doi: 10.2118/17708-MS.

Blasingame, T.A., McCray, T.L., and Lee, W.J. 1991. Decline curve analysis for variable pressure drop/variable flowrate systems. Paper SPE-21513-MS presented at the SPE Gas Technology Symposium, Houston, Texas, USA, January 1991. doi: 10.2118/21513-MS.

Bourgeois, C., Pehlke, T., McQueen, A., and Cashin, D. 2026. Frac optimization: Analyzing operational metrics that matter. Paper SPE-230623-MS presented at the SPE Hydraulic Fracturing Technology Conference and Exhibition, The Woodlands, Texas, USA, February 2026. doi: 10.2118/230623-MS.

Bowie, B., and Ewert, J. 2020. Numerically enhanced RTA workflow: Improving estimation of both linear flow parameter and hydrocarbons in place. Paper URTeC-2020-2967-MS presented at the SPE/AAPG/SEG Unconventional Resources Technology Conference, Virtual, July 2020. doi: 10.15530/urtec-2020-2967.

Brown, M., Ozkan, E., Raghavan, R., and Kazemi, H. 2011. Practical solutions for pressure-transient responses of fractured horizontal wells in unconventional shale reservoirs. *SPE Reservoir Evaluation & Engineering* 14 (6): 663–676. doi: 10.2118/125043-PA.

Carslaw, H.S. and Jaeger, J.C. 1959. *Conduction of heat in solids*, 2nd ed. Oxford: Clarendon Press.

Cipolla, C., Wolters, J., McKimmy, M., Miranda, C., Hari-Roy, S., Kechemir, A., and Gupta, N. 2022. Observation lateral project: Direct measurement of far-field drainage. Paper SPE-209164-MS presented at the SPE Hydraulic Fracturing Technology Conference and Exhibition, The Woodlands, Texas, USA, February 2022. doi: 10.2118/209164-MS.

Clarkson, C.R. 2021. *Unconventional reservoir rate-transient analysis*. Houston, Texas: Gulf Professional Publishing.

Fowler, G., McClure, M., and Cipolla, C. 2019. A Utica case study: The impact of permeability estimates on history matching, fracture length, and well spacing. Paper SPE-195980-MS presented at the SPE Annual Technical Conference and Exhibition, Calgary, Alberta, Canada, September 2019. doi: 10.2118/195980-MS.

Jongeling, C., Ryan, J., Ponners, C., Wytovich, D., Miller, J., Jackson, J., McClure, M., and Fowler, G. 2024. A physics-based approach to characterize productivity loss in the Haynesville shale. Paper URTeC-2024-4033310-MS presented at the SPE/AAPG/SEG Unconventional Resources Technology Conference, Houston, Texas, USA, June 2024. doi: 10.15530/urtec-2024-4033310.

Lake, L.W. 1989. *Enhanced oil recovery*. Englewood Cliffs, New Jersey: Prentice Hall.

Liang, Y., Meier, H., Srinivasan, K., Tahir, H., Ortega, A., Amalokwu, K., Friedrich, J., Okpala, J., Decker, K., Brown, M., Benish, T., Crozier, H., Bhargava, P., Sumant, P., and Reavis, J. 2022. Accelerating development optimization in the Bakken using an integrated fracture diagnostic pilot. Paper URTeC-2022-3719696-MS presented at the SPE/AAPG/SEG Unconventional Resources Technology Conference, Houston, Texas, USA, June 2022. doi: 10.15530/urtec-2022-3719696.

Mattar, L. and McNeil, R. 1998. The "flowing" gas material balance. *Journal of Canadian Petroleum Technology* 37 (2): 52–55.

McClure, Mark, Charles Kang, Chris Hewson, Soma Medam, Egor Dontsov, Ankush Singh, Carlo Peruzzo, and Elizaveta Gordeliy. 2025. ResFrac Technical Writeup. 18th Edition. arXiv:1804.02092.
McClure, M., Kang, C., Hewson, C., Medam, S., Dontsov, E., Singh, A., Peruzzo, C., and Gordeliy, E. 2025. ResFrac technical writeup, 18th ed. Available at arXiv:1804.02092.

McClure, M., Ratcliff, D., Singh, A., Ponners, C., and Fowler, G. 2024. Practical guidelines for DFIT interpretation using the compliance method procedure. Available at arXiv:1804.02092.

McClure, M., Bammidi, V., Cipolla, C., Cramer, D., Martin, L., Savitski, A., Sobernheim, D., and Voller, K. 2019. A collaborative study on DFIT interpretation: Integrating modeling, field data, and analytical techniques. Paper URTeC-2019-123-MS presented at the SPE/AAPG/SEG Unconventional Resources Technology Conference, Denver, Colorado, USA, July 2019. doi: 10.15530/urtec-2019-123.

Morsy, S., Abbott, C., Almasoodi, M., Baldwin, A., Babazadeh, M., Cipolla, C., Elliott, K., Garbino, A., Lassek, J., McKimmy, M., Ponners, C., Shahri, M., Zaghloul, J., and McClure, M. 2025. Blind testing simulator predictions of refracturing performance in the Bakken and the Permian Basin. Paper URTeC-2025-4245581-MS presented at the SPE/AAPG/SEG Unconventional Resources Technology Conference, Houston, Texas, USA, June 2025. doi: 10.15530/urtec-2025-4245581.

Ozkan, E., Brown, M., Raghavan, R., and Kazemi, H. 2011. Comparison of fractured horizontal well performance in tight sand and shale reservoirs. *SPE Reservoir Evaluation & Engineering* 14 (3): 248–259. doi: 10.2118/121290-PA.

Pearson, C.M., Green, C.A., Milton-Tayler, D., and Trevino, V. 2023. Extended-time conductivity testing of proppants at 0.5 lb/ft^2 used for slickwater multistage horizontal completions. Paper SPE-212334-MS presented at the SPE Hydraulic Fracturing Technology Conference and Exhibition, The Woodlands, Texas, USA, January 2023. doi: 10.2118/212334-MS.

Ponners, C., Babazadeh, M., Cipolla, C., Dhuldhoya, K., Lu, Q., Manchanda, R., Tamayo, D.R., Smith, S., Shahri, M., and McClure, M. 2024. Interference testing in shale: A generalized “degree of production interference” (DPI) and developing new insights into the Chow pressure group (CPG). Paper URTeC-2024-4053742-MS presented at the SPE/AAPG/SEG Unconventional Resources Technology Conference, Houston, Texas, USA, June 2024. doi: 10.15530/urtec-2024-4053742.

Raghavan, R. 1976. Well test analysis for wells producing by solution gas drive. *SPE Journal* 16 (4): 196–208.

Raterman, K., Liu, Y., and Warren, L. 2019. Analysis of a drained rock volume: An Eagle Ford example. Paper URTeC-2019-263-MS presented at the SPE/AAPG/SEG Unconventional Resources Technology Conference, Denver, Colorado, USA, July 2019. doi: 10.15530/urtec-2019-263.

Singh, A., Babazadeh, M., Cipolla, C., Dhuldhoya, K., Gandomkar, A., Lassek, J., Manchanda, R., McKimmy, M., Ramirez-Tamayo, D., Safari, R., Shahri, M., Smith, S., and McClure, M. 2025. Far-field drainage along hydraulic fractures: Insights from integrated modeling studies in the Bakken and Permian Basin. Paper SPE-223567-MS presented at the SPE Hydraulic Fracturing Technology Conference and Exhibition, The Woodlands, Texas, USA, February 2025. doi: 10.2118/223567-MS.

Ugueto, G., Wu, K., Jin, G., Zhang, Z., Haffener, J., Shahri, M., Ratcliff, D., Bohn, R., Chavarria, A., Wu, Y., Guzik, A., Srinivasan, A., Gibson, R., and Savitski, A. 2023. A catalogue of fiber optics strain-rate fracture driven interactions. Paper SPE-212370-MS presented at the SPE Hydraulic Fracturing Technology Conference and Exhibition, The Woodlands, Texas, USA, January 2023. doi: 10.2118/212370-MS.

Uzun, I., Kurtoglu, B., and Kazemi, H. 2016. Multiphase rate-transient analysis in unconventional reservoirs: Theory and application. *SPE Reservoir Evaluation & Engineering* 19 (4): 560–572. doi: 10.2118/171657-PA.

Wattenbarger, R.A., El-Banbi, A.H., Villegas, M.E., and Maggard, J.B. 1998. Production analysis of linear flow into fractured tight gas wells. Paper SPE-39931-MS presented at the Rocky Mountain Regional/Low-Permeability Reservoirs Symposium, Denver, Colorado, USA, 5–8 April. doi: 10.2118/39931-MS.

Appendix A

Total Fluid here is defined as the water phase plus the oil phase. Define the phase LFP for oil (LFP_o) and water (LFP_w) as:

$$LFP_o = A_f\sqrt{k_{abs}k_{ro}} \quad \text{(A-1)}$$

$$LFP_w = A_f\sqrt{k_{abs}k_{rw}} \quad \text{(A-2)}$$

There is not necessarily a single, unique way to define the Total-Fluid LFP (LFP_{ow}). One option is to define it as:

$$LFP_{ow} = A_f\sqrt{k_{eff,ow}} = A_f\sqrt{k_{abs}k_{r\_eff}} \quad \text{(A-3)}$$

Where $k_{eff,ow} = k_{abs}k_{r\_eff} = k_{abs}\lambda_t\ \mu_t = k_{abs}(k_{ro} + k_{rw})$.

Here, λ_t is the total mobility and μ_t is the effective/average viscosity.

Therefore, when Equation (A-3) is squared, we get:

$$LFP_{ow}{}^2 = \left(A_f\sqrt{k_{eff,ow}}\right)^2 = \left(A_f\sqrt{k_{abs}(k_{ro} + k_{rw})}\right)^2 = A_f{}^2 k_{abs}k_{ro} + A_f{}^2 k_{abs}k_{rw}$$

$$LFP_{ow} = \sqrt{LFP_o{}^2 + LFP_w{}^2} \quad \text{(A-4)}$$

After converting the surface flow rates to reservoir flow rates, the ratio of the fractional flow of oil and water can be calculated by taking the ratio of the reservoir flow rates of oil and water. Then the ratio of relative permeabilities can be calculated from (Aziz and Settari, 1979; Lake, 1989; Uzun et al., 2016):

$$k_{ro}/_{krw} = \frac{\mu_o}{\mu_w}\frac{f_o}{f_w} \quad \text{(A-5)}$$

Then, from knowledge of LFP_{ow} and $k_{ro}/_{krw}$, it is possible to calculate LFP_o and LFP_w:

$$LFP_{ow}{}^2 = A_f^2 k_{abs}(k_{rw} + k_{ro}) = A_f^2 k_{abs}k_{rw}\left(1 + \frac{k_{ro}}{k_{rw}}\right) = LFP_w^2\left(1 + \frac{k_{ro}}{k_{rw}}\right) = LFP_o^2\left(\frac{k_{rw}}{k_{ro}} + 1\right) \quad \text{(A-6)}$$

$$LFP_w^2 = \frac{LFP_{ow}^2}{1 + k_{ro}/k_{rw}} = \frac{LFP_{ow}^2}{1 + \frac{\mu_o f_o}{\mu_w f_w}} \quad \text{(A-7)}$$

$$LFP_o^2 = \frac{LFP_{ow}^2}{1 + k_{rw}/k_{ro}} = \frac{LFP_{ow}^2}{1 + \frac{\mu_w f_w}{\mu_o f_o}} \quad \text{(A-8)}$$